Metal Hydride Heat Pumps for Upgrading Spacecraft Waste Heat

Hae-Jin Choi* and Anthony F. Mills†
University of California, Los Angeles, Los Angeles, California 90024

Spacecraft waste heat may be upgraded using a metal hydride heat pump. Thermodynamic analysis is used to choose suitable hydride pairs and to estimate system efficiency; promising reductions in radiator weight are indicated. To investigate whether such reductions can be realized in practice, the dynamic response of two coupled hydride beds is modeled accounting for heat transfer, absorption kinetics, and hydrogen flow. Parametric calculations are reported for the $Mg_{2.4}Ni/LaNi_{4.9}Al_{0.1}$ pair, which show an optimal cycle time of 10 ~ 12 min. Actual radiator weight savings prove to be substantially less than thermodynamic analysis estimates. Use of hydride heat pumps shows possible merit only in the case of high sink temperatures when using hardened radiators.

Nomenclature

$\mathscr{A}$ = high-temperature hydride bed
A = area
A_c = cross-sectional area of bed
$\mathscr{B}$ = low-temperature hydride bed
c_b = specific heat of hydride bed
COP = coefficient of performance
COP_C = Carnot cycle coefficient of performance
c_{pg} = constant pressure specific heat of hydrogen
D^* = diffusion parameter
E_a = activation energy for hydrogen diffusion through hydride phase
E_{H_2} = internal energy of hydrogen in the passage
h_c = convective heat transfer coefficient
k_b = thermal conductivity of the bed
K_{eff} = effective Darcy permeability
Kn = Knudsen number
L = bed thickness
M = mass
$\dot{m}$ = hydrogen flow rate
Mg = molecular weight of hydrogen
m_g = total amount of hydrogen transfer
m_r = mass of unit area of radiator
P = hydrogen pressure
P_{eq} = equilibrium pressure
$\mathscr{P}$ = perimeter of bed
$\dot{Q}$ = heat rate
$\mathscr{R}$ = universal gas constant
$\dot{r}$ = reaction rate
T = temperature
T_s = effective sink temperature
t = time
u = superficial velocity of hydrogen
w = hydrogen concentration ratio
x = useful hydrogen capacity
z = axial coordinate

Greek Symbols

ΔH = heat of formation of hydride
ΔS = entropy change of formation of hydride
Θ = dimensionless temperature $[= (T - T_l)/(T_h - T_l)]$
ϵ = emissivity
ϵ_b = packed bed void fraction
η = overall radiator efficiency
μ = viscosity
ρ = density
σ = Stefan-Boltzmann constant
τ_{cycle} = cycle time

Subscripts

A = high-temperature hydride bed $\mathscr{A}$
Aux = auxiliary part
B = low-temperature hydride bed $\mathscr{B}$
H_2 = hydrogen in the passage
h = high
he = heat engine
hp = heat pump
l = low
m = middle
r = radiator
t = total system with use of a heat pump
to = total system without use of a heat pump

Received Nov. 16, 1989; revision received April 24, 1990.

*Research Associate, School of Engineering and Applied Science.
†Professor, School of Engineering and Applied Science.

I. Introduction

SPACECRAFT power levels have risen to 10 kW and are predicted to attain 100 kW or higher.[1] Waste heat is rejected to space by radiators. Reduction of radiator size and weight to lower the launching cost of a spacecraft is desirable, and heat pumps are a possible means to upgrade waste heat temperature for this purpose. The radiator size reduction and associated weight saving may offset the added penalties of the weight and complexity of the heat pump.[1] Grossman[2] presents sample calculations for a $LiBr/H_2O$ absorption heat pump and suggests that absorption heat pumps are promising for space applications. The few moving parts provide for high reliability and long lifetime, and they can be powered by waste heat instead of electricity. However, liquid absorption heat pumps may be difficult to operate at zero gravity, and use of a solid absorbent is attractive. Metal hydride heat pumps can be used over a much wider temperature range than conventional liquid or solid absorption heat pump systems. The major difficulties associated with the use of metal hydrides are the hydrogen content capacity limitation, which is less than 2% by weight; a low thermal conductivity; and inadequate reaction kinetics data for many candidate hydrides.

The first step in the design of a metal hydride heat pump is the selection of a suitable pair of hydrides. A thermodynamic analysis was made to determine the ideal performance of a metal hydride heat pump system. The necessary thermodynamic properties have been tabulated by Dantzer and Orgaz[3]

for 27 candidate metal alloys.These data allow the determination of the maximum operating temperature range for a given pair of alloys, and for a chosen temperature range, a thermal balance yields the coefficient of performance of the cycle. Specification of the cycle time then allows the hydride bed weight to be determined. The next step is to choose a bed configuration and to determine an effective bed thickness that will minimize the cycle time. Previous work, e.g., Ref. 4, has shown that heat transfer to/from the bed and hydrogen flow in/out of the bed are probably the rate limiting processes because of the fast kinetics, low-hydride thermal conductivity, and small hydride particle size (order of microns). An appropriate model has been reported by Choi and Mills.[5] Using this model, a computer program was developed to study the dynamic behavior of coupled hydride beds. Parametric calculations to determine optimal design parameters for a metal hydride heat pump are reported.

II. Thermodynamic Analysis

Figure 1 shows a schematic configuration of spacecraft thermal control by a thermally driven heat pump. Two sources of waste heat are considered; one is high-temperature waste heat from a power generation system at about 700 K, and the other is low-temperature waste heat from electronic devices, etc., at about 300 K. Two radiators are needed to reject this waste heat and to operate at different temperature levels. A thermally driven heat pump run between these two different temperatures will reduce the total radiator area, which is one of the largest and heaviest components of the thermal system.

The heat rejection from flat plate radiators in space can be calculated from

$$\dot{Q}_r = \epsilon\eta\sigma A_r(T_r^4 - T_s^4) \tag{1}$$

Here the overall radiator efficiency η is the ratio of energy rejected to that for an isothermal radiator. In Earth orbit, an effective sink temperature T_s can be used and is defined as the temperature reached by an imaginary surface when it is in thermal equilibrium with its environment. In unfavorable low Earth orbits, effective sink temperatures as high as 270 K have been calculated, but usual values are in the range of 200 to 255 K.[1]

The total radiator area A_{to}, without the use of a heat pump, is the sum of the high-temperature radiator area A_h, and the low-temperature radiator area A_l:

$$A_{to} = A_h + A_l = \frac{\dot{Q}_h}{\epsilon\eta\sigma(T_h^4 - T_s^4)} + \frac{\dot{Q}_l}{\epsilon\eta\sigma(T_l^4 - T_s^4)} \tag{2}$$

When the heat pump is used, the total radiator area is

$$A_t = A_{mA} + A_{mB} = \frac{\dot{Q}_{mA}}{\eta\epsilon\sigma(T_{mA}^4 - T_s^4)} + \frac{\dot{Q}_{mB}}{\eta\epsilon\sigma(T_{mB}^4 - T_s^4)} \tag{3}$$

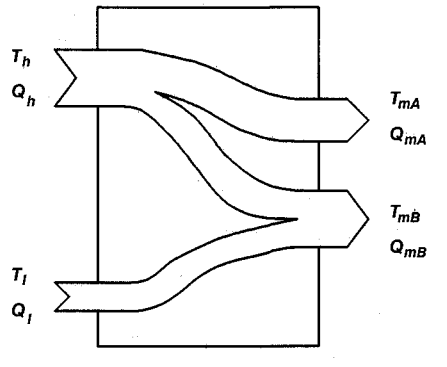

Fig. 1 Thermal diagram for spacecraft waste heat rejection.

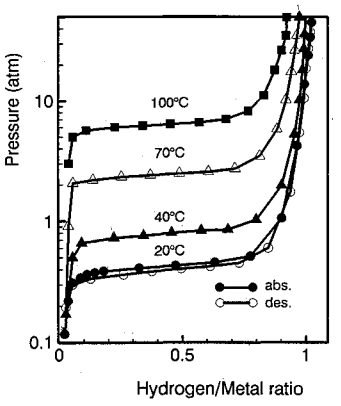

Fig. 2 Hydrogen absorption/desorption isotherms for $LaNi_{4.7}Al_{0.3}$ (annealed for 24 h at 1150°C).[12]

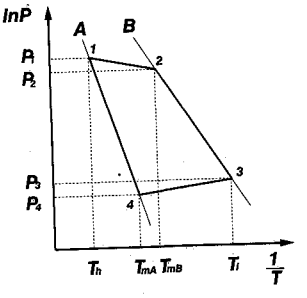

Fig. 3 Cooling cycle of the hydride heat pump on a van't Hoff diagram.

The radiator mass can be assumed roughly linear in radiator area, and the ratio of the total mass of the heat pump system to the original system mass is

$$\frac{M_t}{M_{to}} = \frac{m_r A_t + M_{hp} + M_{Aux}}{m_r A_{to}} = \frac{A_t}{A_{to}} + \frac{M_{hp} + M_{Aux}}{m_r A_{to}} \tag{4}$$

When M_t/M_{to} is less than one, there is merit in using the heat pump for heat rejection.

Characteristic hydride behavior is illustrated in Fig. 2, where absorption and desorption isotherms are shown for several values of temperature. The plateau region, in which there is a relatively small change in pressure with the molar hydrogen/metal ratio, is an important feature for heat pump application. The average pressure over the plateau is given by van't Hoff's equation:

$$\ell n\, P_{H_2} = \Delta H/\mathscr{R}T + \Delta S/\mathscr{R} \tag{5}$$

The heat pump consists of two beds, which are essentially heat exchangers, one filled with the high-temperature hydride $\mathscr{A}$, and the other with the low-temperature hydride $\mathscr{B}$. Figure 3 shows a van't Hoff diagram of two metal hydrides with different P-T relations, which are to be selected as a pair to give the desired operating temperature and pressure ranges. In reality, hydrogen sorption is a dynamic process and equilibrium states will not be achieved during the process. However, a thermodynamic design based on the van't Hoff equilibrium relation is a necessary first step. We will assume that 1) the process is reversible, 2) thermochemical properties are constant, and 3) reactions occur isothermally at a constant plateau pressure without hysteresis.

Referring to Fig. 3 the initial point of the cycle is taken as the high-pressure and high-temperature state; alloy $\mathscr{A}$ is fully hydrided and alloy $\mathscr{B}$ is fully dehydrided. Heat Q_h is supplied to hydride $\mathscr{A}$ at a constant temperature T_h. Hydrogen is transferred from the hydride $\mathscr{A}$ at pressure P_1 to the hydride

$\mathscr{B}$ at P_2 and T_{mB}. The hydrogen release by alloy $\mathscr{A}$ is endothermic ($\mathscr{A}H_x + Q_h \rightarrow \mathscr{A} + H_2$), whereas the hydrogen sorption by alloy $\mathscr{B}$ is exothermic ($\mathscr{B} + H_2 \rightarrow \mathscr{B}H_x + Q_{mB}$). After desorption is complete, alloy $\mathscr{A}$ is cooled from T_h to T_{mA} using an external heat sink. During this "precooling" process, the hydride $\mathscr{B}$ desorbs a certain amount of hydrogen; the required heat of reaction is supplied by the sensible heat capacity of the $\mathscr{B}$ hydride bed, which then cools to T_l with corresponding pressure P_3. Using this low-temperature T_l, the heat of reaction Q_l is absorbed from the cooling load as the hydride $\mathscr{B}$ releases hydrogen ($\mathscr{B}H_x + Q_l \rightarrow \mathscr{B} + H_2$). The hydrogen is transferred from $\mathscr{B}$ to $\mathscr{A}$ where the heat of reaction Q_{mA} is given up to a heat sink at temperature T_{mA}. After desorption from bed $\mathscr{B}$ is complete, bed $\mathscr{A}$ is preheated to temperature T_h, while bed $\mathscr{B}$ absorbs a small amount of hydrogen: the heat of reaction given up heats bed $\mathscr{B}$ to temperature T_{mB}. The cycle thus consists of four steps: 1) hydrogen transfer at high pressure, $1 \rightarrow 2$; 2) precooling; $1 \rightarrow 4$ for $\mathscr{A}$, $2 \rightarrow 3$ for $\mathscr{B}$; 3) hydrogen transfer at low pressure, $3 \rightarrow 4$; and 4) preheating; $4 \rightarrow 1$ for $\mathscr{A}$, $3 \rightarrow 2$ for $\mathscr{B}$.

A. Thermodynamic Calculations

The thermal capacities of heat exchangers and other components are not included in the thermodynamic analysis; also the pressure drop required to transfer the hydrogen is neglected. The energy balance equations are

$$Q_h = \Delta Q(\mathscr{A}H_x) + m_A c_b(\mathscr{A}H_x) \cdot (T_h - T_{mA}) \tag{6}$$

$$Q_{mA} = \Delta Q(\mathscr{A}) + m_A c_b(\mathscr{A}) \cdot (T_{mA} - T_h) + m_g c_{pg} \cdot (T_{mA} - T_l) \tag{7}$$

$$Q_{mB} = \Delta Q(\mathscr{B}) + m_B c_b(\mathscr{B}) \cdot (T_{mB} - T_l) + m_g c_{pg} \cdot (T_{mB} - T_h) \tag{8}$$

$$Q_l = \Delta Q(\mathscr{B}H_x) + m_B c_b(\mathscr{B}H_x) \cdot (T_l - T_{mB}) \tag{9}$$

where the heat of formation of hydride is $\Delta Q(I) = m_g\, \Delta H(I)$, I = alloy $\mathscr{A}$,$\mathscr{B}$, hydride $\mathscr{A}H_x$,$\mathscr{B}H_x$.

The Carnot cycle efficiency for reversible operation is the maximum efficiency attainable for given operating conditions and is a function of working temperatures only.

$$\mathrm{COP}_C = (Q_l/Q_h) = (\mathrm{COP_{he}})(\mathrm{COP_{ref}}) = (W/Q_h) \cdot (Q_l/W)$$

Hence

$$\mathrm{COP}_C = [(T_h - T_{mA})/T_h] \cdot [T_l/(T_{mB} - T_l)] \tag{10}$$

The actual COP of the cycle is simply

$$\mathrm{COP} = Q_l/Q_h \tag{11}$$

For one cycle, Eq. (9) can be written as

$$Q_l = \Delta Q(\mathscr{B}H_x) + m_B c_b(\mathscr{B}H_x) \cdot (T_l - T_{mB}) \tag{12}$$

$$= m_B[x_B\, \Delta H(\mathscr{B}H_x) + c_b(\mathscr{B}H_x)(T_l - T_{mB})] \tag{13}$$

where x_B is the hydrogen capacity of hydride bed $\mathscr{B}$.

$$m_B = \frac{(\text{cooling capacity})(\tau_{\text{cycle}})}{[x_B\, \Delta H(\mathscr{B}H_x) + c_b(\mathscr{B}H_x)(T_l - T_{mB})]} \tag{14}$$

$$m_A = m_B \frac{x_B}{x_A} = \frac{x_B(\text{cooling capacity})(\tau_{\text{cycle}})}{x_A[x_B\, \Delta H(\mathscr{B}H_x) + c_b(\mathscr{B}H_x)(T_l - T_{mB})]} \tag{15}$$

where the cooling capacity is Q_l/τ_{cycle}. The total mass of the hydride beds is

$$m_A + m_B = \frac{(x_A + x_B)(\text{cooling capacity})(\tau_{\text{cycle}})}{x_A[x_B\, \Delta H(\mathscr{B}H_x) + e_b(\mathscr{B}H_x)(T_l - T_{mB})]} \tag{16}$$

Thus the system weight is directly proportional to mass for unit power, cycle time, and cooling capacity. If a cycle time is specified, the hydride bed weights can be calculated. However, to determine an optimum cycle time, a heat and mass transfer analysis of the beds is required.[6]

For space application, the system must satisfy the special temperature range requirements. A single-stage system was chosen and required to upgrade low-temperature waste heat at about 300 K, using high-temperature waste heat at about 700 K. T_{mA} and T_{mB} are fixed values at given T_h and T_l to match equilibrium pressures and can be calculated from Eq. (5). Several possible combinations for the operating temperature range were found from the 27 candidate alloys.[3] Table 1 shows results of thermodynamic calculations. The total weight of the cooling system on a spacecraft is dominated by the low-temperature waste heat radiator. Thus the amount by which the temperature difference can be boosted by the heat pump is the major factor determining the benefit of using a heat pump. Hydride heat pumps can raise the low-temperature waste heat by around 80 K by a single stage, which is a high value for sorption-type heat pumps.

Table 1 Sample combinations for hydride heat pump

Selected couples	T_h	T_{mA}	T_{mB}	T_l	COP	$\frac{\mathrm{COP}}{\mathrm{COP}_C}$
$Mg_{2.4}Ni/LaNi_{4.95}Mn_{0.05}$	670.0	537.7	384.3	300.0	0.25	0.357
$Mg_{2.4}Ni/LaNi_{4.9}Al_{0.1}$	670.0	533.1	387.9	300.0	0.26	0.371
$Mg_{2.4}Ni/LaNi_5$	670.0	543.8	379.8	300.0	0.26	0.366
$Mg(LaNi_5)_{20\%}/LaNi_{4.9}Al_{0.1}$	630.0	563.4	346.0	300.0	0.33	0.478

Table 2 Radiator area and mass saving ratios for hydride heat pumps

		T_s, K			
Selected pairs		100	200	250	275
$Mg_{2.4}Ni/LaNi_{4.95}Mn_{0.05}$	A_t/A_{to}	0.739	0.647	0.474	0.300
	M_t/M_{to}	0.973	0.842	0.605	0.377
$Mg_{2.4}Ni/LaNi_{4.9}Al_{0.1}$	A_t/A_{to}	0.726	0.635	0.464	0.293
	M_t/M_{to}	0.946	0.818	0.587	0.365
$Mg_{2.4}Ni/LaNi_5$	A_t/A_{to}	0.739	0.651	0.481	0.307
	M_t/M_{to}	0.961	0.835	0.605	0.380
$Mg(LaNi_5)_{20\%}/LaNi_{4.9}Al_{0.1}$	A_t/A_{to}	0.831	0.758	0.601	0.415
	M_t/M_{to}	1.03	0.922	0.779	0.479

For sample calculations, a hardened radiator is used for heat rejection, with unit mass of $m_r = 20\ \text{kg/m}^2$. The cycle time of the heat pump is assumed to be 10 min, and the auxiliary system weight is taken as 5 kg/kW. Table 2 shows the thermodynamic calculation results for the area and mass saving ratio with selected hydride couples and several possible effective sink temperatures. When the sink temperature is high, significant savings are obtained in the radiator area and system weight. Ideal cycle operation requires an infinite cycle time. In a real system, a long cycle time causes low power output, whereas a short cycle time reduces the system performance. An optimum cycle time exists that minimizes the total system weight including the radiator and the heat pump.

III. Coupled Hydride Beds

The potential to use metal hydride heat pumps for upgrading spacecraft waste heat was shown by the thermodynamic analysis. However, the dynamic behavior of coupled hydride beds must be studied to evaluate the validity of the thermodynamic analysis and to identify the factors that limit system performance. Several attempts have been made to analyze the coupled hydride bed problem. Mayer et al.[7] attempted to obtain the pressure variation in coupled reaction beds and estimated the gross operating behavior. But, they used an improper hydrogen flow model that assumed no pressure contribution to the flow and ideal mass transfer in beds. Bjurström and Suda[8] used a lumped capacity thermal model to investigate the dynamics of hydrogen transfer between coupled hydride beds and made comparisons with experimental data. The results showed discrepancies in hydrogen flow rate and bed temperatures at short operating times, i.e., less than 10 min. The lumped capacity model is invalid for this high Biot number heat conduction problem. Nagel et al.[9,10] carried out extensive experiments on the dynamic behavior of paired metal hydrides and concluded that considerable deviations exist between dynamic *P-T-C* relations and those under static conditions that are predicted from thermodynamic data.

A. Physical Model

Figure 4 shows two hydride beds and a connecting passage. The system pressure and temperature are determined by ambient temperature conditions, which are usually controlled by changing the flow of the secondary coolant with sets of control valves. A planar bed model is selected for simplicity. Hydrogen is transferred through one side of the slab, and the heat is supplied or removed through the other. The two different reactions occur simultaneously, one in each hydride bed. Thus, the boundary conditions of each hydride bed are strongly coupled and are not the same as those for a single reaction bed under controlled pressure or mass flow rate conditions. Ideal heat source and sink conditions are used giving constant wall temperatures. This assumption is reasonable when heat pipes are used for heating and cooling hydride beds. Hydrogen flow friction is ignored, and the passage is modeled as a perfectly mixed control volume.

Table 3 Hydride heat pump cooling cycle

Step	$\mathscr{A}$ bed	$\mathscr{B}$ bed
Heating	Isothermal heating (des.) $T\|_{z=0} = T_h$	Isothermal heat rejection (abs) $T\|_{z=0} = T_{mB}$
Precooling	Sensible cooling	Adiabatic cooling
	(abs) $T\|_{z=0} = T_{mA}$	(des.) $\left.\dfrac{\partial T}{\partial z}\right\|_{z=0} = 0$
Cooling	Isothermal heat rejection (abs) $T\|_{z=0} = T_{mA}$	Isothermal cooling (des.) $T\|_{z=0} = T_l$
Preheating	Sensible heating	Adiabatic heating
	(des.) $T\|_{z=0} = T_h$	(abs) $\left.\dfrac{\partial T}{\partial z}\right\|_{z=0} = 0$

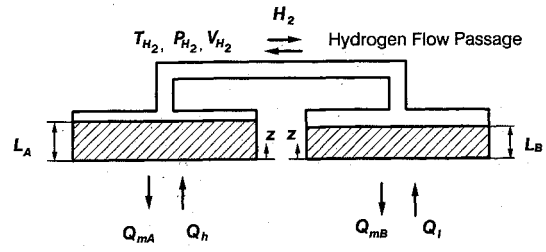

Fig. 4 Schematic configuration of a hydride heat pump.

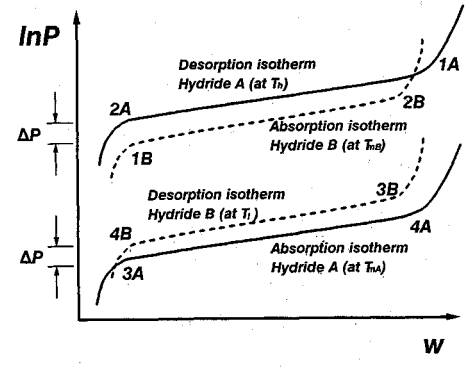

Fig. 5 Hydride heat pump cooling cycle.

The actual sequence of operation is as follows. Figure 5 shows a low-temperature boosting heat pump cycle, plotted on a pressure/hydrogen concentration ratio diagram. Hysteresis exists between the absorption and desorption plateau pressure, and the plateau pressures are not constant while the hydrogen/metal ratio varies. Solid lines indicate the hot side hydride $\mathscr{A}$, and the dotted lines represent the cold side hydride $\mathscr{B}$. Line 1A–2A and 3B–4B are desorption lines and 3A–4A and 1B–2B are absorption lines and show the hysteresis and plateau slope effects. In the thermodynamic analysis, the hydrogen is transferred between the $\mathscr{A}$ bed and the $\mathscr{B}$ bed at the same pressure, given by the van't Hoff equation. However, the reaction driving force is the difference between the hydrogen gas pressure and the equilibrium pressure, which is related to temperature by the van't Hoff equation. The higher pressure difference ΔP guarantees a shorter cycle time, but the system performance will be decreased due to the associated temperature variation. The proper pressure difference should be determined by considering absorption/desorption hysteresis, and plateau slope, both of which lower the pressure difference. Here, the hydrogen pressure in the connecting passage maintains a value that is determined by the energy and mass balances for the two beds. Nagel et al.[9,10] call this pressure the dynamic pressure and the van't Hoff's equilibrium pressure the static pressure. The actual reaction driving force is the pressure difference between the dynamic pressure and the equilibrium pressure of each hydride bed and is called the dynamic pressure difference. Table 3 shows the cyclic operation of the hydride heat pump.

The cycle time is an important parameter of the performance of the system. The cyclic operation of this system is obtained by switching temperature conditions of the hydride beds from T_h to T_{mA} and T_{mA} to T_h and from T_{mB} to T_l and T_l to T_{mB}, respectively. T_{mA} and T_{mB} can be determined by Eq. (5) when T_h and T_l are given.

B. Numerical Simulation Model

A numerical model for the dynamic behavior of the coupled hydride beds has been developed. It is based on a

quasisteady hydrogen flow equation and an unsteady heat-transfer equation with appropriate boundary conditions, namely

$$\frac{\mathrm{d}}{\mathrm{d}z}\left(\frac{K_{\mathrm{eff}}M}{\mu\mathscr{R}T}P\frac{\mathrm{d}P}{\mathrm{d}z}\right)=\dot{r}(z,t) \tag{17}$$

$$(1-\epsilon_b)\rho_b c_b\frac{\partial T}{\partial t}=k_b\frac{\partial^2 T}{\partial z^2}-\rho_g u c_{pg}\frac{\partial T}{\partial z}+\dot{r}(z,t)\,\Delta H \tag{18}$$

$$\dot{r}(z,t)=D^*\exp\left(-\frac{E_a}{\mathscr{R}T}\right)\frac{(P^{1/2}-P_{\mathrm{eq}}^{1/2})}{[(1-w)^{-1/3}-1]} \tag{19}$$

while the boundary conditions are

$$z=L: P=P_0, \qquad -k_b\frac{\partial T}{\partial z}=\rho_g u c_{pg}(T_0-T) \tag{20}$$

$$z=0: T=T_0, \qquad \frac{\mathrm{d}P}{\mathrm{d}z}=0 \tag{21}$$

A mass balance on the hydrogen passage gives

$$(\dot{m}/A_c)_A=\rho_g u|_{z_A=0}=\int_0^{L_A}\dot{r}\,\mathrm{d}z \tag{22}$$

$$(\dot{m}/A_c)_B=\rho_g u|_{z_B=0}=\int_0^{L_B}\dot{r}\,\mathrm{d}z \tag{23}$$

$$\frac{\mathrm{d}m_{\mathrm{H_2}}}{\mathrm{d}t}=-\dot{m}_A-\dot{m}_B \tag{24}$$

The energy balance on the hydrogen passage assumes perfectly insulated walls of zero heat capacity

$$\frac{\mathrm{d}E_{\mathrm{H_2}}}{\mathrm{d}t}=(\dot{m}c_{pg}T_{\mathrm{H_2}})_{\mathrm{in}}-(\dot{m}c_{pg}T_{\mathrm{H_2}})_{\mathrm{out}} \tag{25}$$

and the outside pressure of each bed is assumed to be the same as the pressure in hydrogen passage: the pressure drop in the gas passage is neglected.

$$P_A|_{z=L_A}=P_B|_{z=L_B}=P_{\mathrm{H_2}} \tag{26}$$

Further details of the model and numerical methods may be found in Refs. 5 and 6.

C. Results and Discussion

The $Mg_{2.4}Ni/LaNi_{4.9}Al_{0.1}$ pair was chosen for detailed calculations because the reaction kinetics data of the two hydrides are relatively well known, and these hydrides are appropriate to the required temperature range. In addition, they have good thermodynamic characteristics, namely, a small plateau slope and small hysteresis. Enhanced thermal conductivity beds were used with a nominal effective thermal conductivity of 5 W/m K. The hardened radiator parameters were $m_r = 20$ kg/m^2, $\epsilon = 0.8$, and $\eta = 0.9$. The auxiliary parts of the heat pump were taken to have a mass of $m_{\mathrm{Aux}} = 5$ kg/kW. The specific application selected in this work was to upgrade waste heat in low Earth orbit at $T_l = 300$ K by high temperature waste heat at $T_h = 673$ K. The rejection temperatures were taken to be $T_{mA} = 500$ K and $T_{mB} = 375$ K. The required kinetics parameters in the shrinking core model, Eq. (19), were established as follows: for $Mg_{2.4}Ni$, the parameter D^* was set equal to 70.5 based on the work of Han and Lee.[11] The kinetic parameter of $LaNi_{4.7}Al_{0.3}$, $D^* = 175$ was used for $LaNi_{4.9}Al_{0.1}$ because no suitable kinetic data could be found. All thermodynamic properties were based on the work by Dantzer and Orgaz[3] and Huston and Sandrock.[12] Property values used are tabulated in Table 4.

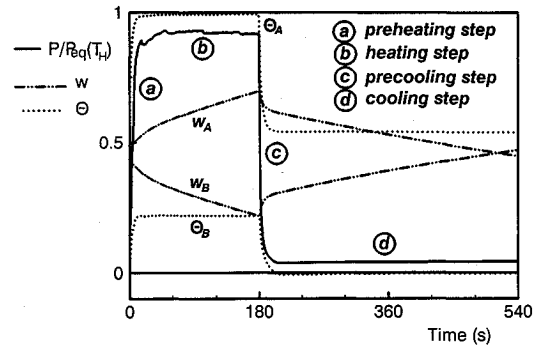

Fig. 6 Pressure, average bed temperature and average hydrogen concentration profiles of $Mg_{2.4}Ni/LaNi_{4.9}Al_{0.1}$ pair hydride heat pump.

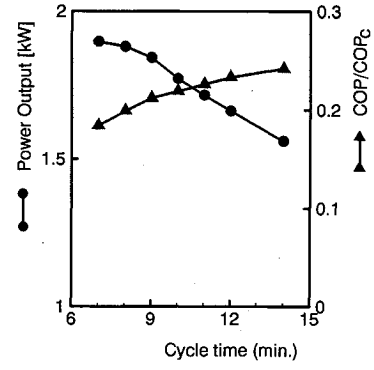

Fig. 7 Effect of cycle time on the system COP/COP$_C$ and power output.

Table 4 $Mg_{2.4}Ni/LaNi_{4.9}Al_{0.1}$ heat pump properties used for the numerical calculations[3,11,12]

		$\mathscr{A}$ bed, $Mg_{2.4}Ni$	$\mathscr{B}$ bed, $LaNi_{4.9}Al_{0.1}$
ϵ_b	Void fraction	0.5	0.5
ρ_b	Density, kg/m^3	1000.0	2540.0
c_α	Heat capacity of α phase, J/kg K	664.4	335.8
c_β	Heat capacity of β phase, J/kg K	936.3	501.6
d_p	Average particle diameter, μm	3.0	3.0
L	Bed thickness, mm	10.0	10.0
$m_{\mathscr{A},\mathscr{B}}$	Bed weight, kg	27.7	25.4
k_b	Thermal conductivity, W/m K	5.0	5.0
ω_0	Initial hydrogen content	0.45	0.45
$[H/M]_{\max}$	Hydrogen capacity, $\mathrm{mol_H/mol_{alloy}}$	1.5	6.0
$\mathrm{d}(\ell n\, P)/\mathrm{d}\omega$	Slope of plateau region	0.034	0.126
$\ell n(P_a/P_d)$	Pressure hysteresis	0.1	0.093
D^*	Kinetic parameter, kg/s m^2 N$^{1/2}$	70.5	175.0

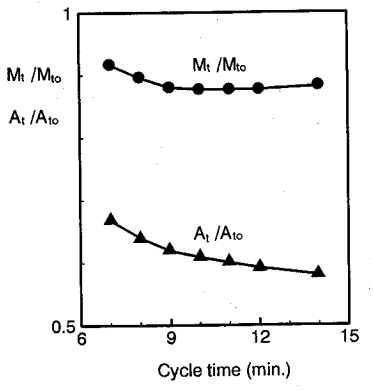

Fig. 8 Radiator mass and area saving ratio as a function of cycle time.

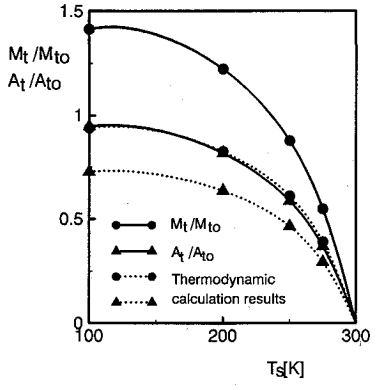

Fig. 9 Effect of sink temperatures on radiator mass and area saving ratio: cycle time is 10 min.

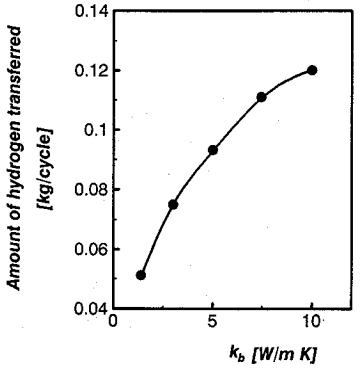

Fig. 10 Amount of hydrogen transferred as a function of the effective thermal conductivity of hydride bed matrix.

Figure 6 shows the system pressure and the average bed temperature changes with time for one cycle. The pressure and temperature variations are periodic and are almost constant for the heating and cooling steps. Abrupt changes exist for the preheating and precooling steps. Experimental data show smoother curves for these steps[7] because rapid changes of the wall temperature are prevented by the effect of the auxiliary system thermal mass, which is not accounted for in the numerical model.

In the heating step, the hydrogen concentration ratios change quickly: the slope is steep. But the ratios vary slowly in the cooling step. This means that the reaction kinetics are faster in the high-pressure operating process and slow in the low-pressure operating process. From the single bed analysis,[5] we know that hydrides have fast reaction kinetics and the heat transfer limitation is the rate limiting step. However, high-temperature hydrides that operate in a high-temperature region have a large activation energy E_a. The reaction rate is related to temperature by Arrhenius' law, Eq. (19): a high temperature increases the reaction rate exponentially, and the activation energy determines the slope of the reaction rate variation with changing inverse temperature. The high-temperature hydride has fast reaction kinetics in the high-temperature region, but the reaction rate decreases rapidly with temperature due to the large activation energy. In the high-pressure operating region, the high-temperature hydride $\mathscr{A}$ has faster reaction kinetics than the low-temperature hydride $\mathscr{B}$, and the rate limitation can be the heat transfer in the $\mathscr{B}$ bed. However, in the low-pressure operating region, the $\mathscr{A}$ bed has a quite low reaction rate, and these reaction kinetics become the rate limiting processes: the hydrogen desorbed from the $\mathscr{B}$ bed cannot be absorbed into the $\mathscr{A}$ bed rapidly enough, and the cooling step controls the overall performance.

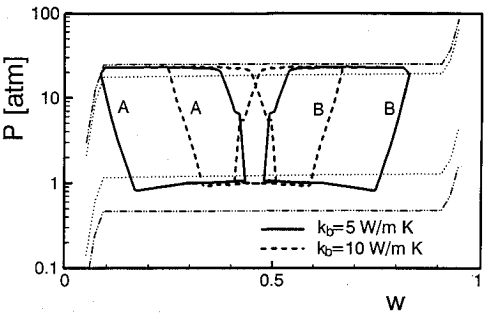

Fig. 11 Dynamic hydrogen pressure as a function of hydrogen concentration ratio: cycle time of 10 min.

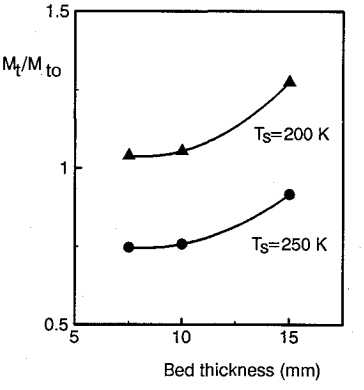

Fig. 12 Effect of bed thickness on the total radiator mass savings: $k_{eff} = 10$ W/mK and a cycle time of 10 min.

The influence of the cycle time on the system performance and the power output is illustrated in Fig. 7. A higher COP and lower cooling power were obtained with a longer cycle time. When the cycle time is increased, the system performance increases and the total radiator area is decreased, whereas the cooling output is reduced and the required heat pump weight for unit cooling load is increased. This indicates that an optimal cycle time exists to minimize the total system weight, which includes the radiator weight, heat pump weight, and auxiliary plumbing weight. To enhance the hydrogen transfer rate, a shorter period was taken for a faster reaction step, and a longer period was used for a slower reaction step, so as to match the total amount of hydrogen transferred. It was found that 3 min are sufficient for the heating step, but a longer time was needed to obtain the necessary hydrogen transfer during the cooling step. In practice, the cooling time will have to be the same or a multiple of the heating time for continuous operation.

Figure 8 shows the total mass and radiator area saving ratio as a function of cycle time at $T_s = 250$ K. The area reduction ratio decreased monotonically from a value of 0.668

for a 7-min cycle time to a value of 0.580 for 14 min. The saving ratio shows that an optimum cycle has a mass saving ratio about 0.877 for an 11-min cycle time.

The area and mass reduction ratios at different effective sink temperatures are shown in Fig. 9. It is observed that large savings are obtained in the radiator area at all sink temperatures, but no gain was found in the total weight savings at sink temperatures less than 230 K. There are large discrepancies between the simulation results and thermodynamic calculation results. In the thermodynamic calculation, 75% of hydrogen is transferred, but in reality only about 25% of hydrogen is transferred due to the limitation of reaction kinetics.

Figure 10 shows the amount of hydrogen transferred as a function of the effective thermal conductivity of the hydride bed matrix. A substantial improvement in the amount of hydrogen transferred is found up to a value of about 10 W/m K. From the single bed analysis,[5] little further improvement of hydrogen transferred was expected above a value of 5 W/m K. However, a significant increase still exists above 5 W/m K. This feature can be explained using Fig. 11, which shows the relations of hydrogen dynamic pressure to hydrogen content ratio. The actual dynamic pressure is different from the static pressure given by the vant' Hoff equilibrium relation and is located between the expected static pressures of coupled hydrides. The cyclic diagram shows counterclockwise operation for the $\mathscr{A}$ bed and clockwise operation for the $\mathscr{B}$ bed. For coupled bed operation, the locations and the shapes of the diagram in the P vs w coordinate are determined by the reaction rates in the two beds. The width of the diagrams show the amount of hydrogen transferred: wider diagrams are required for higher performance. The locations indicate the rate limiting step in an operating cycle. When the reaction rates of the heating and cooling steps are matched, the diagrams are located in the center and form a cycle at the same location of hydrogen content ratio w. Solid lines show this case. Dashed lines show the results for an effective thermal conductivity of 10 W/m K. The $\mathscr{A}$ bed works with a low hydrogen content and the $\mathscr{B}$ bed operates within a high hydrogen content range. Notice that the sorption rate is a function of the temperature, pressure, and hydrogen concentration ratio w. A low hydrogen content implies a high reaction rate, as given by Eq. (19). Thus the increase of thermal conductivity eliminates not only the heat-transfer limitation of the hydride beds, but also the reaction kinetics limitation of the high-temperature hydride bed $\mathscr{A}$ during the cooling step. This is an interesting phenomenon for high-temperature hydride heat pumps, and it can be used for improving the system performance.

Figure 12 shows the effect of bed thickness. The dynamic analysis of the $Mg_{2.4}Ni/LaNi_{4.9}Al_{0.1}$ pair heat pump showed that heat transfer was not the dominant limitation, and reaction kinetics were the rate limiting processes. As the bed thickness increases, there is more alloy available for absorbing hydrogen, but the weight of the bed increases for a unit heat exchanger surface, and the effect of the pressure drop in the hydrogen flow causes a decrease of reaction driving force in Eq. (19). This analysis only takes the hydride bed weight into account. The optimum bed thickness may be larger than indicated by Fig. 12 when the weight of the heat exchanger surface and coolant plumbing is considered.

The hydrogen content capacity limitation, which is less than 2.0 wt% in general, is one of the major restrictions to the use of hydride heat pumps, and it is the high-temperature hydride that has the smaller capacity. More research is required to improve undesirable hydride properties, in particular the hydrogen content capacity and thermal conductivity. Calculations showed that an increase of $(H/M)_{\max,A}$ from 1.5 to 3.0, results in a decrease of the hydride bed weight from 20.0 to 16.0 kg/kW.

IV. Conclusions

Thermodynamic analysis shows that the use of metal hydride heat pumps to upgrade spacecraft waste heat has considerable potential for reducing radiator weight, which may offset the added penalties of the weight and complexity of the heat pump. However, numerical simulation of the dynamic response of two coupled hydride beds, accounting for heat transfer, hydrogen flow, and reaction kinetics, gave less promising results. Parametric calculations for the $Mg_{2.4}Ni/LaNi_{4.9}Al_{0.1}$ hydride pair show the following.

1) The sorption kinetics of the high-temperature hydride $Mg_{2.4}Ni$ is the rate limiting process.

2) An optimal cycle time is about $10 \sim 12$ min.

3) Augmentation of thermal conductivity up to about 10 W/m K leads to a significant improvement of the system performance. Enhanced thermal conductivity increases not only heat transfer but also the sorption rates of the rate limiting hydride bed.

4) A significant difference exists between thermodynamic calculations and complete simulation, primarily due to the rate limiting sorption kinetics.

5) A large reduction in radiator area can be achieved. But the merit in using hydride heat pump is questionable, due to the system weight, particularly when the sink temperatures are lower than about 220 K.

Acknowledgments

This work was supported by the San Jose State University Foundation on subcontract 057-6. The Principal Investigator was D. K. Edwards, Department of Mechanical Engineering, University of California, Irvine. Computer time was supplied by the Campus Computing Network of the University of California, Los Angeles.

References

[1]Dexter, P. F., and Haskin, W. L., "Analysis of Heat Pump Augmented System for Spacecraft Thermal Control," AIAA Paper 84-1757, June 1984.

[2]Grossman, G., "Heat Pump Systems for Enhancement of Heat Rejection from Spacecraft," *Analysis and Applications of Heat Pumps, the Winter Annual Meeting of the ASME*, American Society of Mechanical Engineers, Chicago, Nov.–Dec. 1988, pp. 85–95.

[3]Dantzer, P., and Orgaz, E., "Thermodynamics of Hydride Chemical Heat Pump—II. How to Select a Pair of Alloys," *International Journal of Hydrogen Energy*, Vol. 11, No. 12, 1986, pp. 797–806.

[4]Supper, W., Groll, M., and Mayer, U., "Reaction Kinetics in Metal Hydride Reaction Beds with Improved Heat and Mass Transfer," *Journal of Less-Common Metals*, Vol. 104, 1984, pp. 279–286.

[5]Choi, H., and Mills, A. F., "Heat and Mass Transfer in Metal Hydride Beds for Heat Pump Application," *International Journal of Heat and Mass Transfer*, Vol. 33, No. 6, 1990, pp. 1281–1288.

[6]Choi, H., "Hydride Heat Pumps for Upgrading Spacecraft Waste Heat," Ph.D. Dissertation, School of Engineering and Science, Univ. of California, Los Angeles, 1989.

[7]Mayer, U., Groll, M., and Supper, W., "Heat and Mass Transfer in Metal Hydride Reaction Beds: Experimental and Theoretical Results," *Journal of Less-Common Metals*, Vol. 131, 1987, pp. 235–244.

[8]Bjurström, H., and Suda, S., "The Metal Hydride Heat Pump: Dynamics of Hydrogen Transfer," *International Journal of Hydrogen Energy*, Vol. 14, No. 1, 1989, pp. 19–28.

[9]Nagel, M., Komazaki, Y., and Suda, S., "Dynamic Behaviour of Paired Metal Hydrides: I. Experimental Method and Results," *Journal of Less-Common Metals*, Vol. 120, 1986, pp. 45–53.

[10]Nagel, M., Komazaki, Y., Matsubara, Y., and Suda, S., "Dynamic Behaviour of Paired Metal Hydrides: II. Analytical Survey of the Experimental Results," *Journal of Less-Common Metals*, Vol. 123, 1986, pp. 47–58.

[11]Han, J. S., and Lee, J. Y., "A Study on the Dehydriding Kinetics of Mg_2Ni Intermetallic Compound," *Journal of Less-Common Metals*, Vol. 128, 1987, pp. 155–165.

[12]Huston, E. L., and Sandrock, G. D., "Engineering Properties of Metal Hydrides," *Journal of Less-Common Metals*, Vol. 74, 1980, pp. 435–443.